Imaging Ca^{2+} Entering the Cytoplasm through a Single Opening of a Plasma Membrane Cation Channel

Hui Zou,* Lawrence M. Lifshitz,*‡ Richard A. Tuft,*‡ Kevin E. Fogarty,*‡ and Joshua J. Singer*

From the *Department of Physiology and ‡Biomedical Imaging Group, University of Massachusetts Medical School, Worcester, Massachusetts 01655

abstract Discrete localized fluorescence transients due to openings of a single plasma membrane Ca^{2+} permeable cation channel were recorded using wide-field digital imaging microscopy with fluo-3 as the Ca^{2+} indicator. These transients were obtained while simultaneously recording the unitary channel currents using the whole-cell current-recording configuration of the patch-clamp technique. This cation channel in smooth muscle cells is opened by caffeine (Guerrero, A., F.S. Fay, and J.J. Singer. 1994. *J. Gen. Physiol.* 104:375–394). The localized fluorescence transients appeared to occur at random locations on the cell membrane, with the duration of the rising phase matching the duration of the channel opening. Moreover, these transients were only observed in the presence of sufficient extracellular Ca^{2+}, suggesting that they are due to Ca^{2+} influx from the bathing solution. The fluorescence transient is characterized by an initial fast rising phase when the channel opens, followed by a slower rising phase during prolonged openings. When the channel closes there is an immediate fast falling phase followed by a slower falling phase. Computer simulations of the underlying events were used to interpret the time course of the transients. The rapid phases are mainly due to the establishment or removal of Ca^{2+} and Ca^{2+}-bound fluo-3 gradients near the channel when the channel opens or closes, while the slow phases are due to the diffusion of Ca^{2+} and Ca^{2+}-bound fluo-3 into the cytoplasm. Transients due to short channel openings have a "Ca^{2+} spark-like" appearance, suggesting that the rising and early falling components of sparks (due to openings of ryanodine receptors) reflect the fast phases of the fluorescence change. The results presented here suggest methods to determine the relationship between the fluorescence transient and the underlying Ca^{2+} current, to study intracellular localized Ca^{2+} handling as might occur from single Ca^{2+} channel openings, and to localize Ca^{2+} permeable ion channels on the plasma membrane.

key words: calcium • caffeine-activated channel • nonselective cation channels • fluo-3 fluorescence • smooth muscle

INTRODUCTION

Ca^{2+} plays a crucial role in a variety of cellular biochemical and physiological processes. The application of Ca^{2+}-sensitive fluorescent indicators and the development of imaging technology have greatly advanced our ability to understand the mechanisms involved in global and, more recently, localized Ca^{2+} handling. Localized Ca^{2+} signaling is of particular importance because not only can the generation of a highly localized intracellular Ca^{2+} pulse regulate such physiological events as exocytosis and ion channel activation, but it can also affect resting Ca^{2+} levels and contribute to global elevations of Ca^{2+}, and consequently affect distant cellular events (see Berridge, 1997; Bootman et al., 1997a; Neher, 1998).

The localized Ca^{2+} transients investigated so far include such "elementary events" as "Ca^{2+} sparks" (Cheng et al., 1993; Nelson et al., 1995; Tsugorka et al., 1995; Klein et al., 1996; Koizumi et al., 1999) and "Ca^{2+} puffs/blips" (Yao et al., 1995; Parker and Yao, 1996; Bootman et al., 1997b; Koizumi et al., 1999) arising from the opening of ryanodine receptors or IP_3 receptors, respectively. Although the fluorescence changes associated with these events are well characterized and the studies of such elementary events have greatly enhanced the understanding of local and global Ca^{2+} signaling, the precise relationship between these fluorescence changes and the channel openings that underlie these events (number of receptors/channels involved, channel kinetics, channel unitary current, etc.) is not clear (see Cannell and Soeller, 1999; Schneider, 1999; Shirokova et al., 1999). To determine this relationship, it would be useful to record the fluorescence transient due to Ca^{2+} influx through a verifiable single channel opening—the "fundamental event" (see Lipp and Niggli, 1996; Berridge, 1997).

Since the amount of Ca^{2+} entry can be determined from the channel unitary current and open time, a

Portions of this work were previously published in abstract form (Zou, H., K.E. Fogarty, R.A. Tuft, and J.J. Singer. 1998. *J. Gen. Physiol.* 111:12a; and Zou, H., L.M. Lifshitz, R.A. Tuft, K.E. Fogarty, and J.J. Singer. 1999. *Biophys. J.* 76:A465).

Address correspondence to Department of Physiology, University of Massachusetts Medical School, 55 Lake Avenue North, Worcester, MA 01655. Fax: 508-856-5997; E-mail: imaging.ionchannels@umassmed.edu

J. Gen. Physiol. © The Rockefeller University Press • 0022-1295/99/10/575/14 $5.00
Volume 114 October 1999 575–588
Available online 27 September 1999
http://www.jgp.org

Ca^{2+}-permeable plasma membrane ion channel would be a good candidate for obtaining such a fundamental event, provided the fluorescence transient can be detected while recording the unitary single channel current. Another advantage of using a plasma membrane ion channel is that the rate of Ca^{2+} entry can be adjusted by altering the driving force for Ca^{2+} via changes in the membrane potential and extracellular Ca^{2+} concentration. Such a channel has been identified and the fluorescence transients associated with single openings of this channel are described in this study.

Previously, a plasma membrane, Ca^{2+} permeable, nonselective cation channel was characterized in toad stomach smooth muscle cells (Guerrero et al., 1994a,b). This channel appears to be directly activated by caffeine; activation does not require changes in membrane potential, intracellular Ca^{2+} concentration, or cyclic AMP levels. In the solutions used for the studies by Guerrero et al. (1994a,b), the caffeine-activated channel conductance is 80 pS and the zero-current potential is near 0 mV. The open times of the channel can be long (longer than 500 ms). Since, under whole-cell current recording conditions, at most ~10–15 channels are open at the same time, the caffeine-activated channel apparently has either a low plasma membrane density or a low probability of being open. These characteristics make it possible to resolve single channel openings in the whole-cell current recording. Using a dual wavelength microfluorimeter to obtain measurements of global Ca^{2+} with fura-2 as the Ca^{2+} indicator, Guerrero et al. (1994b) determined that ~20% of the channel current is carried by Ca^{2+} at −80 mV. Since, at physiological concentrations of extracellular Ca^{2+}, there would be >1 pA Ca^{2+} current (out of >5 pA total current) passing through this channel, we thought that it might be possible to image the fluorescence increase associated with the Ca^{2+} transient that occurs when this channel opens and simultaneously record the (large and long duration) unitary currents. To this end, a wide-field digital imaging microscope was used with fluo-3 as the fluorescent Ca^{2+} indicator to image the distribution of Ca^{2+} in the cell while recording the unitary currents. Thapsigargin and/or ryanodine were used in the experiments to eliminate possible effects of intracellular Ca^{2+} stores.

The results presented here demonstrate the detection of the localized discrete fluorescence transient due to Ca^{2+} entry through a single opening of this caffeine-activated plasma membrane cation channel while simultaneously recording the unitary current. Moreover, the location of the plasma membrane channels can be obtained from the images of the transients. Computer simulations of the events associated with a channel opening were used as an aid to interpret the time course of the observed transients.

MATERIALS AND METHODS

Single Smooth Muscle Cell Preparation

Smooth muscle cells were enzymatically dispersed from the stomach of the toad, *Bufo marinus*, as previously described (Fay et al., 1982; Lassignal et al., 1986) and used on the same day. All experiments were carried out at room temperature.

Patch-Clamp Recordings

Whole-cell currents were recorded with an Axopatch-1D amplifier (Axon Instruments) using standard patch-clamp techniques, and caffeine-activated channel unitary currents were usually recorded with the membrane potential held at −80 mV. After rupturing the patch membrane, 5–10 min elapsed before collecting data to allow the fluo-3 concentration inside the cell to reach a steady level. The membrane potential was sampled at 1 kHz, as was the whole-cell current after the latter was low-pass filtered at 200 Hz.

Ca^{2+} Imaging and Data Processing

Two-dimensional fluorescent Ca^{2+} images were obtained using the Ca^{2+} indicator fluo-3 (50 μM) loaded into the cells through the patch pipette. Fluo-3 was used because of its low background fluorescence and its ~200× fluorescence increase upon binding Ca^{2+} (Harkins et al. 1993). The 488-nm line of an argon-ion visible laser was used as the source of the excitation light. For these studies, fluorescence images were acquired using a custom built high-speed digital imaging microscope (see ZhuGe et al., 1999, for a description of the system). Images were acquired at 15-, 30-, or 50-ms intervals, depending on the purpose of the experiment, with a 6-ms exposure time. A maximum of 200 images could be acquired during any recording sequence at the repetition rates used. In an attempt to catch the entire fluorescence transient associated with the channel opening, a circular-buffer protocol (software provided by Dr. Karl D. Bellvé, Biomedical Imaging Group) was used in some experiments to control image sampling. For this protocol, a circular buffer of 100 images was continuously refreshed once sampling started and the whole-cell current was monitored on an oscilloscope. When a channel opening was observed after caffeine application, manual triggering caused the previous 100 and next 100 images to be saved, so that the whole image set was composed of 200 images. Several image sets were generally obtained from the same cell. The laser shutter control voltage (sampled at 1 kHz) was simultaneously recorded with the current to facilitate the alignment of the fluorescence trace with the corresponding current trace.

Images were processed using custom designed software. Each image is composed of 128 × 128 pixels either 500- or 333-nm square. At each pixel, the fluorescence in the absence of transients (F_0) and during a transient (F) was used to construct the ratio images [F/F_0 or $\Delta F/F_0 = (F - F_0)/F_0$], which were then smoothed (with a 3 × 3 kernel approximating a Gaussian with $\sigma = 1$ pixel) before analysis and display. The resting fluorescence, F_0, was obtained by averaging the fluorescence intensity of 10 consecutive images when there was no fluorescence transient. Each of the fluorescence traces in the figures was obtained from the pixel where the greatest fluorescence change was observed during a localized Ca^{2+} transient. The outline of the cell in the fluorescence ratio images was usually determined by applying a fluorescence intensity threshold. For some of the images, the background was masked using an outline of the cell obtained by manually tracing the fluorescence image. When necessary, to correct for the photo bleaching of fluo-3, the cell fluorescence was normalized to the fluorescence of that part of the cell that did not have any transient activity. A pseudocolor intensity ratio

scale was generated for each set of images and is displayed in each of the figures.

Generally, the focus was adjusted to what appeared to be the center of the cell. Therefore, if the cell was cylindrical in shape and was lying on the bottom of the chamber, then a transient at the edge of the two-dimensional image would be more likely to be in focus. Moreover, the farther the transient was from the edge and the closer it was towards the middle of the cell image (on the top or on the bottom half of the cell), the more likely it would be out of focus (e.g., see Fig. 5). If the diameter of the cell changed with length, or the focal plane was not in the center of the cell, then an in-focus transient might be observed in the middle of the two-dimensional image of the cell. A transient occurring near the middle of the cell image, whether in or out of focus, would be expected to have a smaller amplitude (F/F_0) than one in the same focal plane near the edge of the cell. This occurs mainly because the background resting fluorescence, F_0, would be higher due to the greater thickness at the center of the cell. Therefore, for the same ΔF, F/F_0 is necessarily smaller.

Computer Simulation

To understand the processes underlying the fluorescence images when the channel opens, we simulated the distribution in time and space of free Ca^{2+}, bound and free fluo-3, and bound and free stationary endogenous Ca^{2+} buffers. To do this, finite difference approximations were used to solve a set of partial differential equations for the reaction–diffusion kinetics in a cylindrical coordinate system. This representation, an enhanced version of the simulation by Kargacin and Fay (1991), assumed that the cell was cylindrically symmetric so that the simulation of three-dimensional kinetics required only two coordinates, radius and length, thus significantly reducing the numerical calculations.

Two models of the smooth muscle cell were used. One was a longer cylinder (length = 30 μm, radius = 6 μm) with a channel in the center (see Fig. 4). The other was a shorter cylinder (length = 12 μm, radius = 6 μm) with the channel centered at one end. These simulations were "oriented" relative to an optical axis, and then numerically blurred (convolved) with a point spread function of a microscope (see below). We examined the longer cylinder with its axis perpendicular to the optical axis, and the shorter cylinder with its axis either perpendicular to or aligned with the optical axis. These orientations of the shorter cylinder provided, respectively, a view of the transient with the channel on the side or on the top/bottom of the cell. All three configurations (i.e., the longer cylinder or the shorter cylinder in two orientations) have their advantages and disadvantages. For example, the shorter cylinder with the channel at the end more closely approximates the transient near the channel; i.e., for hemispherical diffusion. On the other hand, the longer cylinder better resembles the shape and basal fluorescence spatial profile of a real smooth muscle cell. However, all three configurations produced qualitatively similar results. Ignoring blurring, the results presented for a channel in the center of the cylinder with a given current are the same as those for a channel at the end of the cylinder with one half that current. For Figs. 4 and 6, the results are shown using the longer cylinder.

For the simulations, the following parameters were used: channel opening of 600 ms with a 1.2-pA Ca^{2+} current; initial free intracellular Ca^{2+} concentration of 100 nM; total endogenous stationary buffer concentration of 230 μM and total fluo-3 concentration of 50 μM; an on-rate of 80 μM/s for fluo-3 and 100 μM/s for the stationary buffer; an off-rate of 90 μM/s for fluo-3 and 100 μM/s for the stationary buffer (yielding a K_d of 1.13 μM for fluo-3 and 1 μM for the stationary buffer); a diffusion constant of 2.5×10^{-6} cm^2/s for Ca^{2+} and 2.2×10^{-7} cm^2 /s for free and Ca^{2+}-bound fluo-3. The effects of plasma membrane pumps and leaks were negligible and no other intracellular activity (e.g., Ca^{2+}-induced Ca^{2+} release, Ca^{2+} uptake) was included. Diffusion, rate and dissociation constants, and the concentration of stationary buffer are from Smith et al. (1998) or Kargacin and Fay (1991).

Images of the intracellular concentrations of the free Ca^{2+}, fluo-3, and Ca^{2+}-bound fluo-3 were typically generated every millisecond. The time intervals used in the simulation were actually much finer to ensure stability of the explicit method used in the finite difference approximation to the partial differential equations. After simulation in a two-dimensional coordinate system at 100-nm spatial resolution, images were converted to three dimensions at the appropriate pixel size (e.g., 333 nm). The Ca^{2+}-bound fluo-3 concentration image was then convolved with the theoretically derived (Tella, 1985) point spread function (oil lens with a NA of 1.3, 530 nm emission) of wide-field and confocal (assuming an infinitely small pinhole) microscopes to mimic the optically blurred observation through the camera. The point spread functions were sharper than those expected from real microscopes. The fluorescence from free fluo-3 was ignored since it is only $\sim$1/200 the brightness of the Ca^{2+}-bound fluo-3. Fluorescence changes over time (F/F_0 or $\Delta F/F_0$) were then extracted from various planes through the cell to determine what would be observed for both in- and out-of-focus transients. For example, the fluorescence change 2 μm above the channel was extracted and plotted together with the in-focus fluorescence change (Fig. 4).

The sensitivity of the results (e.g., predicted F/F_0, estimated Ca^{2+} concentration, etc.) to a variety of parameters was examined by carrying out simulations with various values for cell size, diffusion constants, concentrations of fluo-3 and stationary endogenous buffers, and their on and off rates for Ca^{2+} binding, channel location, and current amplitude. The final values used here were adopted from the literature (Smith et al., 1998; Kargacin and Fay, 1991) to illustrate the basic findings from these simulations and were not meant to be predictive of the values underlying the measured results. A difference between the simulations carried out here and those generally found in the literature dealing with single Ca^{2+} channels is that, because of the long channel openings and the small cell radius, volume limitations were taken into account. Other simulations without these limitations generally follow the diffusion process into an infinite volume (e.g., Naraghi and Neher, 1997; Smith et al., 1998). In addition, theoretical point spread functions were also used here to take into account the optical blurring of the microscope, especially because of the large depth of field of wide-field optics (see also Blumenfeld et al., 1992).

Solutions

In most experiments, 40 μl of cells in dissociation solution were added to a 1.5-ml chamber with a standard bathing solution containing (mM): 127 NaCl, 3 KCl, 1.9 $CaCl_2$, 1 $MgCl_2$, 10 HEPES, pH 7.4. The standard whole-cell patch pipette solution contained (mM): 130 KCl, 1 $MgCl_2$, 20 HEPES, 3 Na_2ATP, 1 Na_3GTP, 0.05 fluo-3 (pentapotassium salt; from Molecular Probes, Inc.), pH 7.2. These solutions differed somewhat from those used by Guerrero et al. (1994a,b), resulting in a slightly larger unitary current at −80 mV. Modifications of the solutions for specific experiments are indicated in the text and figure legends. The free Ca^{2+} concentrations in solutions containing DiBrBAPTA (Molecular Probes, Inc.) were calculated using MAXChelator, a computer program based on the work of Bers et al. (1994). To remove possible effects of intracellular Ca^{2+} stores, for most experiments, thapsigargin (1 or 3 μM; Sigma Chemical Co.) was added to the bathing solution and/or ryanodine (100 μM; Sigma Chemical Co.) was added to the pipette solution. Usually both were

present. The stock solutions for thapsigargin (10 mM) and ryanodine (10 or 100 mM) were in DMSO and stored at −20°C.

The occurrence of caffeine-activated channel openings and associated fluorescence transients does not require the presence of thapsigargin and/or ryanodine since they could be recorded in the absence of these agents (not shown). Moreover, spatially averaged transients correlated with the opening of the caffeine-activated channels without these agents have been described previously (Guerrero et al., 1994a,b).

Caffeine Application

Caffeine (usually 20 mM dissolved in the bathing solution) was applied to the cells by pressure ejection from a micropipette (puffer pipette) using a picospritzer (General Valve Corp.). The ejection pressure, caffeine application time, and the distance between the puffer pipette and the cell were usually adjusted to optimize the recording of single channel openings such that only one or two channels were open at the same time. In general, brief (subsecond) caffeine applications to the cells were repeated before data acquisition to help empty intracellular Ca^{2+} stores and test for the presence of the caffeine-activated channels. Caffeine was applied continuously for 3 s before sealing onto some of the cells, bathed in a thapsigargin-containing solution for at least 15 min, to maximally release Ca^{2+} from intracellular stores (ZhuGe et al., 1999). There was no noticeable difference between the results obtained from these cells and from cells that were not exposed to caffeine for such an extended period of time. In some experiments, two picospritzers were used so that caffeine in different solutions could be applied to the same cell (also see the caption for Fig. 2). The puffer control monitor was sampled at 1 kHz.

RESULTS

Localized Fluorescence Transients Are Observed in Association with Single Channel Openings

Application of caffeine to a smooth muscle cell with the membrane potential held at −80 mV causes inward unitary currents (Fig. 1 B; also Guerrero et al., 1994a). When fluorescence images were acquired while simultaneously recording the unitary currents, discrete, localized, transient fluorescence increases appeared at various times and at various locations throughout the cell. For the cell in Fig. 1, repeated image sets revealed localized transients in at least eleven different locations (Fig. 1 A, a–k). For the current recording shown (Fig. 1 B), with the images acquired every 50 ms, the discrete fluorescence increases were found at eight different locations (Fig. 1 A, a–h). When the fluorescence traces

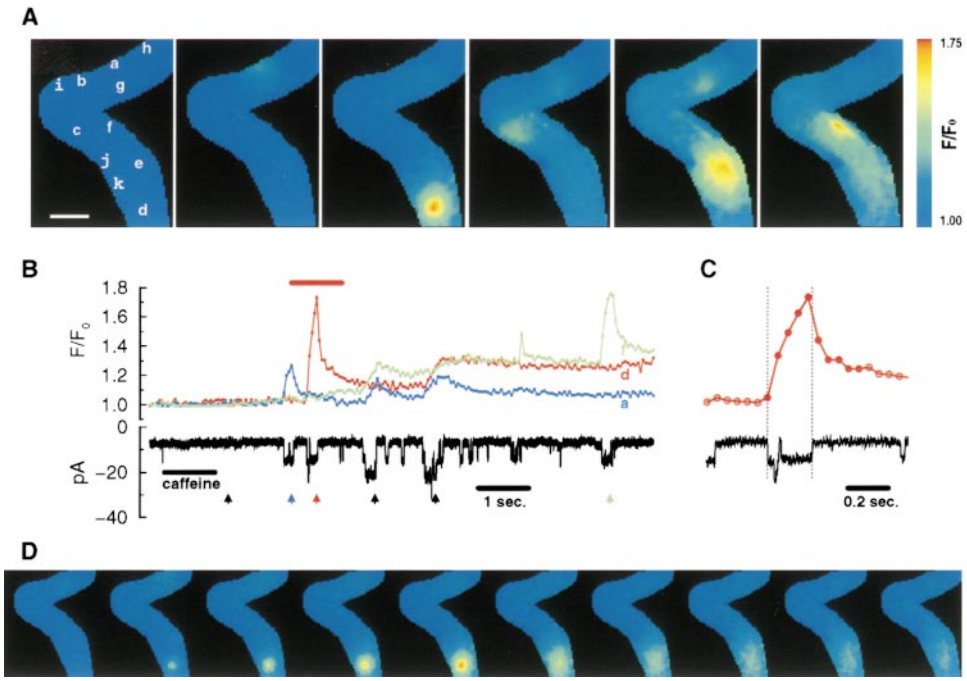

Figure 1. Application of caffeine causes discrete, localized fluorescence transients associated with single openings of plasma membrane cation channels. The fluorescence transients appear to occur at random locations (A) with the duration of their rising phase matching the duration of the channel opening (B and C). The letters in the first image in A indicate the center of each of the discrete fluorescence transients. Therefore, each letter marks the location of a caffeine-activated channel on the plasma membrane. The dots or circles in the fluorescence traces (B and C) indicate when individual images were acquired. The arrows in B correspond, left to right, to the time when each of the selected images in A was acquired. The whole-cell current recording (with the membrane potential held at −80 mV) and the time course of the fluorescence changes at three locations (a, d, and f) are shown in B. To reveal in more detail the correspondence of the local fluorescence changes and the opening and closing of a channel, a segment of d (indicated by the red bar above the trace) along with the current trace are shown on an expanded time scale (C) with the images (D) acquired at the time of the filled circles. Dotted lines define the opening and the final closing of the channel. The brief closure of the channel (for ~12 ms, ~56 ms after it first opened) did not cause a decrease of the fluorescence trace at this time resolution. A brief opening of a different channel (for ~18 ms located far away at h) occurred just before this brief closure (see Fig. 3 for a more straightforward record without brief closures or additional openings from other channels). The transient at d is presumably more in focus than the transients at a, c, and g, which are more diffuse (A). The later slow rise at d (B) is due to the diffusion from a transient that occurred at e. Images were acquired at 50-ms intervals and the pixel size for the images is 500 nm. The relatively larger pixel size and slower image acquisition rate were used here to obtain information regarding the spatial distribution of the transients, as well as the entire fluorescence change associated with each channel opening. The scale bar in A is 10 μm. The format used for A–C is also used for the subsequent figures.

from these locations were aligned in time with the whole-cell current trace (examples for three locations are shown in Fig. 1 B), every one of these fluorescence transients was found to correspond to a single channel opening in the current trace. However, the reverse was not the case since the transients corresponding to some of the channel openings either occurred out of the image field or, less likely, were possibly masked by a nearby transient.

To examine the temporal relationship between the fluorescence transient and the channel opening in more detail, the transient at one location (d) and the corresponding unitary current trace are plotted on an expanded time scale (Fig. 1 C). The 10 sequential images comprising this transient, starting with the one immediately preceding the channel opening, are also shown (Fig. 1 D). When the channel opened, the fluorescence increased from the resting level and continued to rise during the ~200 ms the channel was open. The fluorescence decreased when the channel closed and stayed closed. In the images (Fig. 1 D), the punctate appearance of the fluorescence increase appeared as soon as the channel opened and the fluorescence intensity and spatial spread kept increasing during the time the channel was open. When the channel closed, and therefore the Ca^{2+} source was removed, the local fluorescence declined and became more diffuse with time. These observations suggest that the fluorescence

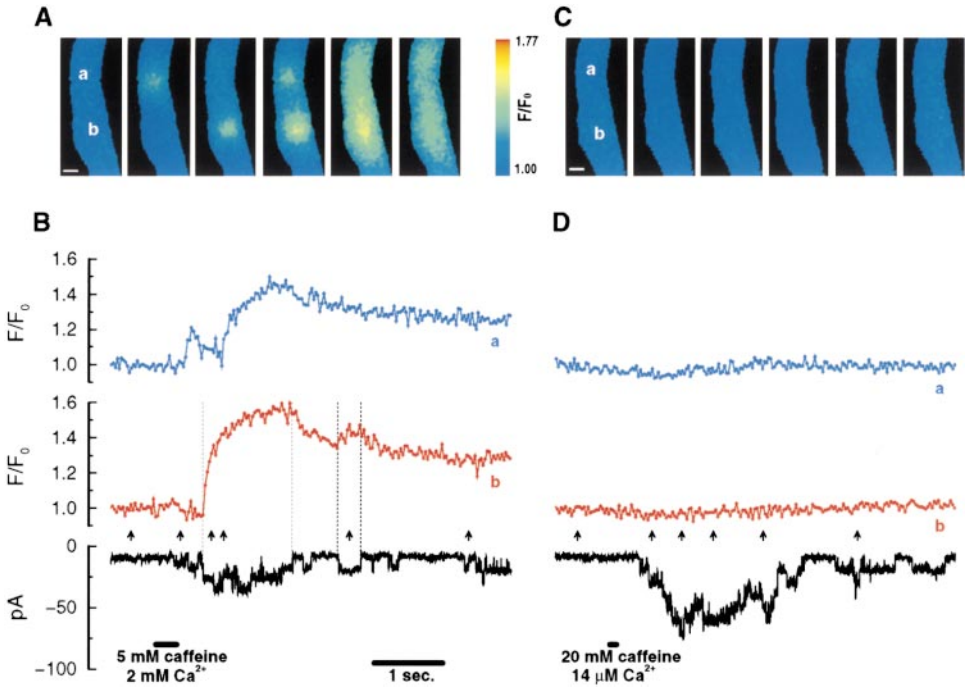

Figure 2. Fluorescence transients were only evident when caffeine-activated channels opened in the presence of sufficient extracellular Ca^{2+}, indicating that the recorded fluorescence transients are due to Ca^{2+} passing through the channels. Cells were bathed in a 14-μM free Ca^{2+} solution. A brief application of 5 mM caffeine dissolved in a 2-mM free Ca^{2+} solution caused the opening of caffeine-activated channels. In the image set shown, fluorescence transients were observed at two different locations in the cell, marked with a and b in the first image in A. The fluorescence changes at these locations are displayed in B along with the current record. The two transients occurring at b corresponded to the two channel openings in the current trace defined by the dotted lines. Approximately 2.5 min after the recording shown in A and B was obtained, 20 mM caffeine was applied to the same cell, but this time dissolved in the 14-μM Ca^{2+} bathing solution. More caffeine-activated channels were opened; however, there were no clear fluorescence transients associated with these openings (C and D). The images in C were selected for the time it would most likely have been possible to record fluorescence transients according to the current trace (D). The fluorescence traces in D are from the two locations (a and b) where the largest fluorescence changes (though minimal compared with the fluorescence traces in B) were detected, and approximately where fluorescence transients were observed previously. Similar results were also obtained when caffeine was applied in these two solutions before the recordings shown in B, in the intervening 2.5 min, and after the recordings in D. With the brief application of the 2-mM Ca^{2+}-containing solution for this experiment, it is quite likely that the extracellular Ca^{2+} concentration (a) declined during the time course of the recording, and (b) varied spatially at any one time in the immediate vicinity of the cell. The first can explain why the second opening of the same channel (B) is associated with a smaller than expected fluorescence transient in b and a larger unitary current (the channel conductance is larger in solutions containing lower Ca^{2+} concentrations; Guerrero et al. 1994a). The second can explain the different amplitudes of the unitary currents occurring at about the same time; for example, the first and the second openings in the current trace. However, the possibility of the occurrence of channel subconductance states under these experimental conditions cannot be ruled out. The basal fluorescence intensity is much lower in these cells bathed in solutions containing low Ca^{2+} concentrations. Therefore, for the same amount of Ca^{2+} entry, the increase in fluorescence (F/F_0 or $\Delta F/F_0$) would be greater. A puffer pipette with a larger opening and containing 5 mM caffeine was used for the 2-mM Ca^{2+} solution to ensure that while a large part of the cell would be exposed to 2 mM Ca^{2+}, the caffeine concentration was relatively low so that only a few channel openings would occur. On the other hand, to maximize the chance of seeing a transient in the 14-μM Ca^{2+} solution, the usual concentration of caffeine (20 mM) was used. Pixel size for the images is 333 nm, and the images were acquired every 30 ms. The scale bars are 5 μm in A and C. The 14-μM free Ca^{2+} solution contained (mM): 127 NaCl, 3 KCl, 1 $MgCl_2$, 2 $CaCl_2$, 2.5 DiBrBAPTA, 10 HEPES, 0.001 thapsigargin, pH 7.4. The 2-mM free Ca^{2+} solution contained (mM): 127 NaCl, 3 KCl, 2 $CaCl_2$, 1 $MgCl_2$, 10 HEPES, pH 7.4.

transient was following the Ca^{2+} influx through a single opening of the caffeine-activated plasma membrane cation channel located in a particular area of the cell membrane. Because of its punctate appearance and steep spatial gradient, this transient was most likely more in focus than some of the other transients, which had a more diffuse appearance (Fig. 1 A). Since each and every observed transient corresponded to a single channel opening, the location of the transient revealed the location of the channel on the plasma membrane (projected onto these two-dimensional images). Although not rigorously studied, it appears that caffeine-activated channels are not localized in any one particular region of the cell, but rather seem randomly distributed over the cell surface. It is unlikely that intracellular Ca^{2+} stores contributed to these transients since the bathing and pipette solutions contained thapsigargin and ryanodine, respectively.

The Localized Fluorescence Transients Are Due to Ca^{2+} Entry through Single Channel Openings

If the fluorescence transients described above were indeed due to Ca^{2+} entry through the caffeine-activated channels, then they would be expected to be abolished when the channels open in a bathing solution where the Ca^{2+} concentration is sufficiently reduced. To see if this would be the case, cells were bathed in a solution in which the Ca^{2+} concentration was lowered to ~14 μM, which should substantially decrease the fraction of the unitary current carried by Ca^{2+} (Fig. 2). Application of caffeine dissolved in this bathing solution activated the channels; however, no clear fluorescence transients were detected (in any of the 38 image sets from five cells, with at least 5 image sets per cell). When caffeine dissolved in a solution containing 2 mM Ca^{2+} was briefly applied to the same cells, discrete fluorescence transients were observed (in 26 of 27 image sets with at least three image sets from each cell showing a transient).

Similar results were also obtained when Ca^{2+} in the bathing solution was buffered to 3.6 μM (2 mM Ca^{2+} and 4 mM DiBrBAPTA) or when the bathing solution contained 200 μM BAPTA and no added Ca^{2+} ("zero Ca^{2+} bathing solution"). No fluorescence increases were observed when the channels were opened by applications of caffeine dissolved in either bathing solution (in all six image sets from two cells in the 3.6 μM Ca^{2+} bathing solution with at least two image sets from each cell; and in all of the 29 image sets from five cells in the zero Ca^{2+} bathing solution with at least four image sets from each cell). However, discrete localized fluorescence transients were evident in the same cells when the channels were opened by applications of caffeine dissolved in a solution containing 2 mM Ca^{2+} (in five of nine image sets in the 3.6 μM Ca^{2+} bathing solution with at least two image sets from each cell showing a transient, and in all 19 image sets in the zero Ca^{2+} bathing solution with at least three image sets from each cell). Therefore, sufficiently reducing the driving force for Ca^{2+} entry by decreasing the Ca^{2+} gradient across the cell membrane abolishes the fluorescence transients. In the zero Ca^{2+} bathing solution, applications of caffeine caused mainly shorter duration channel openings; i.e., longer openings were much less frequent than was the case in the 14 μM Ca^{2+} bathing solution. Chiefly because of the shorter openings in the zero Ca^{2+} bathing solution, the 14 μM Ca^{2+} bathing solution was a better control for demonstrating the requirement for extracellular Ca^{2+}.

Further evidence that these fluorescence transients are due to Ca^{2+} entry was obtained by changing the membrane potential to alter the driving force for Ca^{2+} entry. Fluorescence transients were recorded from the same cell in the standard bathing solution with the cell membrane potential alternately held at −50 and −100 mV. If the fluorescence transients were due to Ca^{2+} entry, they should have a faster initial rate of rise at −100 than at −50 mV because the initial rate of rise (measured as the slope of the initial linear part of the fluorescence change) represents a measurement of the underlying current that is carried by Ca^{2+} (see Fig. 6 and discussion). This current should be larger at −100 than at −50 mV.

There are three factors that complicate these measurements. First, often there were brief closures of the channel that might interrupt the increase of the fluorescence transient. Hence, the measurement for the initial rate of rise could only be obtained up to the time when the first brief closure occurred. Second, for these studies, the images were acquired every 15 ms and the channel opening might occur anytime during this 15-ms period. Therefore, counting only the first data point showing a fluorescence increase after the channel opened could affect the apparent initial rate of rise of the transient. Because of these two factors, the initial rate of rise of a transient was usually measured as the slope of the linear part of the fluorescence trace: between the point immediately preceding channel opening and the fourth point into the transient in the absence of closures, or between the point immediately preceding channel opening and the point immediately preceding the closure if it occurred earlier than the fourth sampling point. Third, the initial rate of rise of each recorded transient depended on how well it was in focus (see below). Therefore, paired comparisons were made between the fluorescence transients at the two membrane potentials at the same location in the cell.

The mean ratio (±SEM) of the initial rate of rise at −100 mV to that at −50 mV was 2.1 ± 0.5, which is significantly greater than 1 (14 different locations in five

cells, $P < 0.01$, two-tailed t test based on the difference between the natural logs of the rates of rise when compared with zero), indicating that fluorescence transients at −100 mV had a greater average initial rate of rise than those from the same location at −50 mV. The temporal order of the holding potential did not appear to affect the measurements. This result is consistent with the generation of a larger Ca^{2+} influx at more negative holding potentials.

In summary, all of these results obtained by altering the driving force on Ca^{2+}, either by changing the extracellular Ca^{2+} concentration or by changing the membrane potential, suggest that the observed localized fluorescence transients are indeed due to Ca^{2+} influx through single openings of a plasma membrane ion channel. These fluorescence transients are associated with increases in the underlying intracellular free Ca^{2+} concentration or single channel Ca^{2+} transients (SCCaTs) and, therefore, can be designated as single channel Ca^{2+} fluorescence transients (SCCaFTs).[1] These terms are analogous to the terms "Ca^{2+} sparks" and "sparks" or "fluorescence sparks" used by Cheng et al. (1993) or Blatter et al. (1997). However, the term "Ca^{2+} sparks" has been used to convey both meanings.

Both the Rise and Fall of SCCaFTs Are Composed of an Initial Fast Phase followed by a Slower Phase

To examine the time course of the rising phase of the SCCaFT in more detail, SCCaFTs were monitored at a higher temporal resolution by acquiring images every 15 ms. For the channel located at the center of the image (Fig. 3), a very long opening without discernible closures occurred after a briefer opening of the same channel. When a long channel opening occurs, especially in the near absence of brief closures with the channel in or nearly in focus, it becomes quite clear that while the channel is open, the SCCaFT is composed of a rapid initial rise followed by a slower rise. Moreover, when the channel closes, the fluorescence decrease is composed of a fast initial phase followed by a slower phase as the fluorescence returns towards its resting level. This time course seems to be characteristic of the SCCaFT as imaged with wide-field optics.

Consistent with two phases for the rise and fall of the transients, neither the rise nor the fall for the long transient in Fig. 3 could be well fit with a single exponential. Instead, the sum of two exponentials was required for a reasonably good fit (Fig. 3, inset). The rise and fall of other transients also appeared to be fit by the sum of two exponentials, but it was difficult to make comparisons because both the degree of focus and the presence of brief closures affect the results.

[1]*Abbreviation used in this paper:* SCCaFT, single channel Ca^{2+} fluorescence transient.

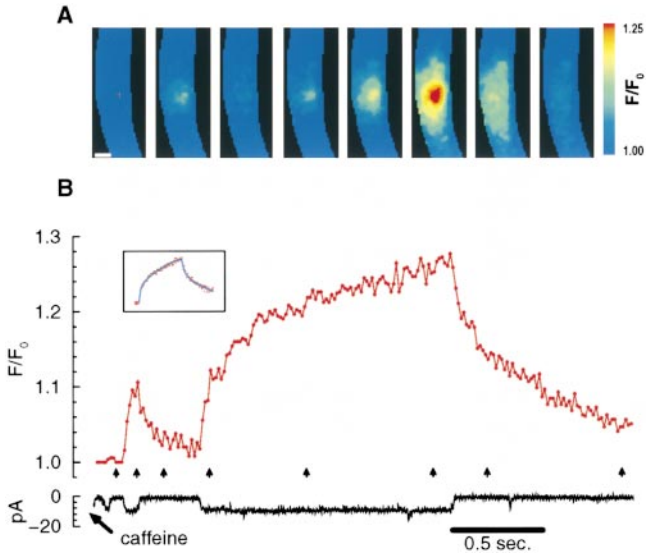

Figure 3. By acquiring images more frequently (every 15 ms), a rapid and a slow phase of fluorescence change was revealed after both the opening and the closing of the channel. A long opening occurred after a short opening of the same channel (determined from the location of the transients in the images). This long opening is especially illustrative of the time course of a SCCaFT because of the apparent absence of any significant brief closures. Shown in the inset are the data fit by the sum of two exponentials for both the rising $\{F/F_0 = 1.10 \cdot [1 - \exp(-t_{rise}/49.5)] + 1.24 \cdot [1 - \exp(-t_{rise}/1{,}130.9)]$, $r^2 = 0.98\}$ and falling $[F/F_0 = 1.08 \cdot \exp(-t_{fall}/72.3) + 1.18 \cdot \exp(-t_{fall}/1{,}051.1)$, $r^2 = 0.95]$ phases (t_{rise} and t_{fall} are in milliseconds). Caffeine was applied for 0.1 s, about 1 s before the beginning of the traces. Pixel size for the images is 500 nm. The scale bar is 5 μm in A.

Computer Simulations Reproduce the Two Phases of a SCCaFT

To understand the time course of the fluorescence transient and the underlying events when a channel opening occurred, we simulated a caffeine-activated channel opening in a smooth muscle cell using a modification of the simulation carried out by Kargacin and Fay (1991). For the simulation described here (Fig. 4), the model cell was cylindrically symmetric, 30-μm long and 12 μm in diameter, with a 1.2-pA unitary Ca^{2+} current (approximately the portion of the current passing through the channel that is carried by Ca^{2+}). Cell dimensions were chosen so that the cell was long enough to eliminate the end-effects that would also be absent with a real cell, while the diameter, close to that of the cells used, would provide the volume effects of the real cell. The channel was located in the center of the cell to simplify calculations. See methods for further details and for the rationale.

From the simulation, it is clear that when the channel opens, Ca^{2+}-bound fluo-3 as well as free Ca^{2+} increase abruptly in the immediate vicinity (<100 nm) of the channel (Fig. 4 B), and each establishes a large spatial gradient. Ca^{2+} (either free or bound to fluo-3) then

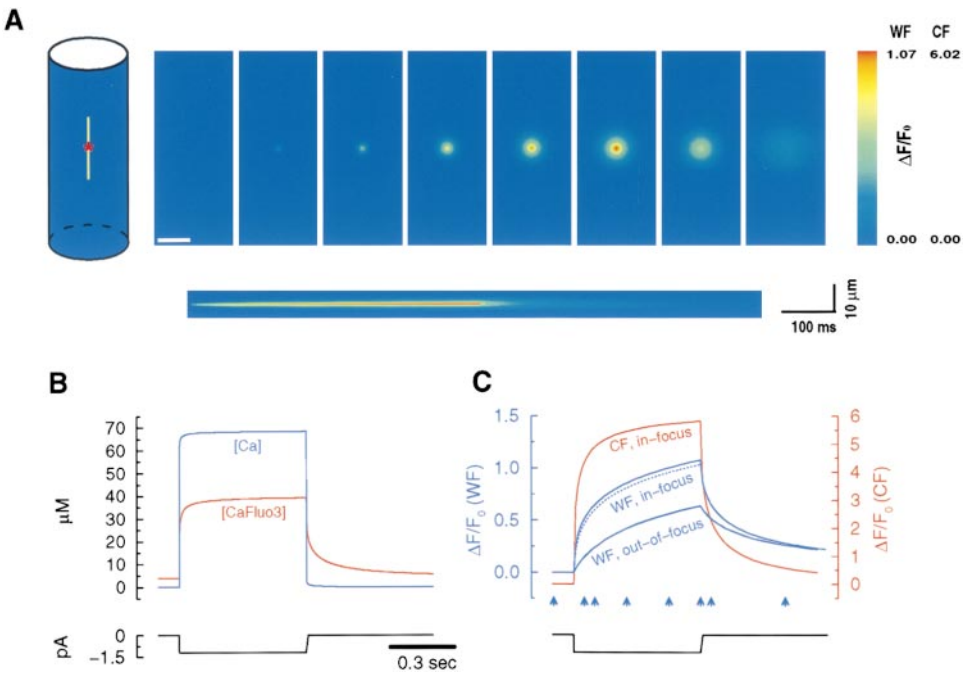

Figure 4. Computer simulations reveal the underlying mechanism causing the observed fluorescence transients. A channel located at the center (*) of a cylindrically symmetrical model cell (A, left) was used to simulate the binding and diffusional events that occur in response to Ca^{2+} entry through a 600-ms opening of a caffeine-activated channel (simulated current traces in B and C; for more details, see methods). A shows a sequence of the blurred wide-field in-focus images produced by the simulation, as well as the fluorescence changes with time from a theoretical line scan that would be obtained from a confocal microscope (the scanning line, 10-μm long with a 100-nm pixel, illustrated in the cell drawing). The calculated free Ca^{2+} and Ca^{2+}-bound fluo-3 concentrations in close vicinity to the channel (100-nm voxel) are shown in B. The corresponding observed fluorescence changes through wide-field (WF) and confocal (CF) optics (blurred with the corresponding theoretical point-spread functions) for in-focus 100-nm pixels are shown in C. The dotted line is the fluorescence trace obtained with a 500-nm pixel from the wide-field image. The fluorescence change obtained from a plane 2 μm above the channel location (mimicking a 2-μm out-of-focus transient) is also shown (C). The arrows in C indicate the time during the simulation when the constructed images (A) were obtained. The scale bar in A is 5 μm.

quickly diffuses away from the channel so that near steady state levels (with a slow rise) are maintained for both Ca^{2+} and Ca^{2+}-bound fluo-3 in the vicinity of the channel. After the channel closes, the three-dimensional diffusion of Ca^{2+} and fluo-3 rapidly abolishes the spatial gradients to establish a homogeneous equilibrium in the cell determined by (in the absence of Ca^{2+} removal mechanisms) the amount of Ca^{2+} entry and the cell volume (Fig. 4 B; see also Stern, 1992; Smith et al., 1998).

To obtain from the simulated data what would be observed with the camera after blurring by the microscope optics, the simulated Ca^{2+}-bound fluo-3 image was convolved with the theoretical point spread function of a wide-field microscope. Similar to what was observed experimentally (Fig. 3), for the pixel overlaying the channel, the fluorescence transient in these blurred images also reveals two distinct phases when the channel opens or when it closes (Fig. 4 C). When the channel opens, the initial rapid rise corresponds to Ca^{2+} entry and the quick establishment of the local near steady state. The slower rise corresponds to the increasing fluorescence farther from the channel as Ca^{2+} and Ca^{2+}-bound fluo-3 are distributed throughout the cell (Fig. 4 A). The optical blurring averages the near-channel fluorescence (i.e., the changes in the Ca^{2+}-bound fluo-3 concentration; Fig. 4 B) with the fluorescence from the accumulation of Ca^{2+}-bound fluo-3 occurring within a larger cell volume. When the channel closes, the sudden removal of the Ca^{2+} source causes the rapid decrease in fluorescence near the channel, while the slower phase represents the processes whereby Ca^{2+} and Ca^{2+}-bound fluo-3 diffuse away from the channel. The in-focus image better reflects the kinetics and amplitude of the rapid phases than the out-of-focus images. As can be seen in the 2-μm out-of-focus fluorescence change in Fig. 4 C, the kinetics are slowed and the amplitude is decreased with defocus. These effects are due to the fact that less of the near-channel fluorescence is being collected in the same size pixel in the out-of-focus image. For comparison, the simulated Ca^{2+}-bound fluo-3 image was also convolved with a theoretical point spread function of a confocal microscope. The blurred line scan image and the fluorescence change from the pixel overlying the channel are displayed in Fig. 4, A and C, respectively.

In-Focus SCCaFTs Are Brighter and Better Reflect the Underlying Channel Behavior than Out-of-Focus SCCaFTs

Characteristics of the in- and out-of-focus fluorescence traces obtained from the simulation are clearly present in the recorded images of relatively in- and out-of-focus SCCaFTs shown in Fig. 5. As the respective channels opened and closed, the in-focus SCCaFT (Fig. 5, A and B) clearly showed two phases and a larger amplitude,

while the out-of-focus SCCaFT (considerably out-of-focus examples are shown in Fig. 5, C and D) was slower in its time course and smaller in amplitude. Moreover, with the out-of-focus SCCaFT, the fast fluorescence changes due to brief closures of the channel became smaller and tended to disappear compared with the large decreases (or "valleys") in fluorescence with the in-focus SCCaFT. Thus, the fluorescence changes of the in-focus SCCaFT have a much stronger correlation with channel openings and closings, indicating that they better represent the Ca^{2+} (or Ca^{2+}-bound fluo-3) changes in the vicinity of the channel. The fast phases are revealed only when imaging with high temporal resolution, even if the transient is relatively in focus (compare to the SCCaFT Fig. 1 C, d). Most recorded SCCaFTs fall between the examples shown in Fig. 5.

In summary, compared with out-of-focus SCCaFTs, in-focus SCCaFTs have a larger fluorescence change and a much more rapid initial rise and fall when the channel opens and closes. Furthermore, the fluorescence of an

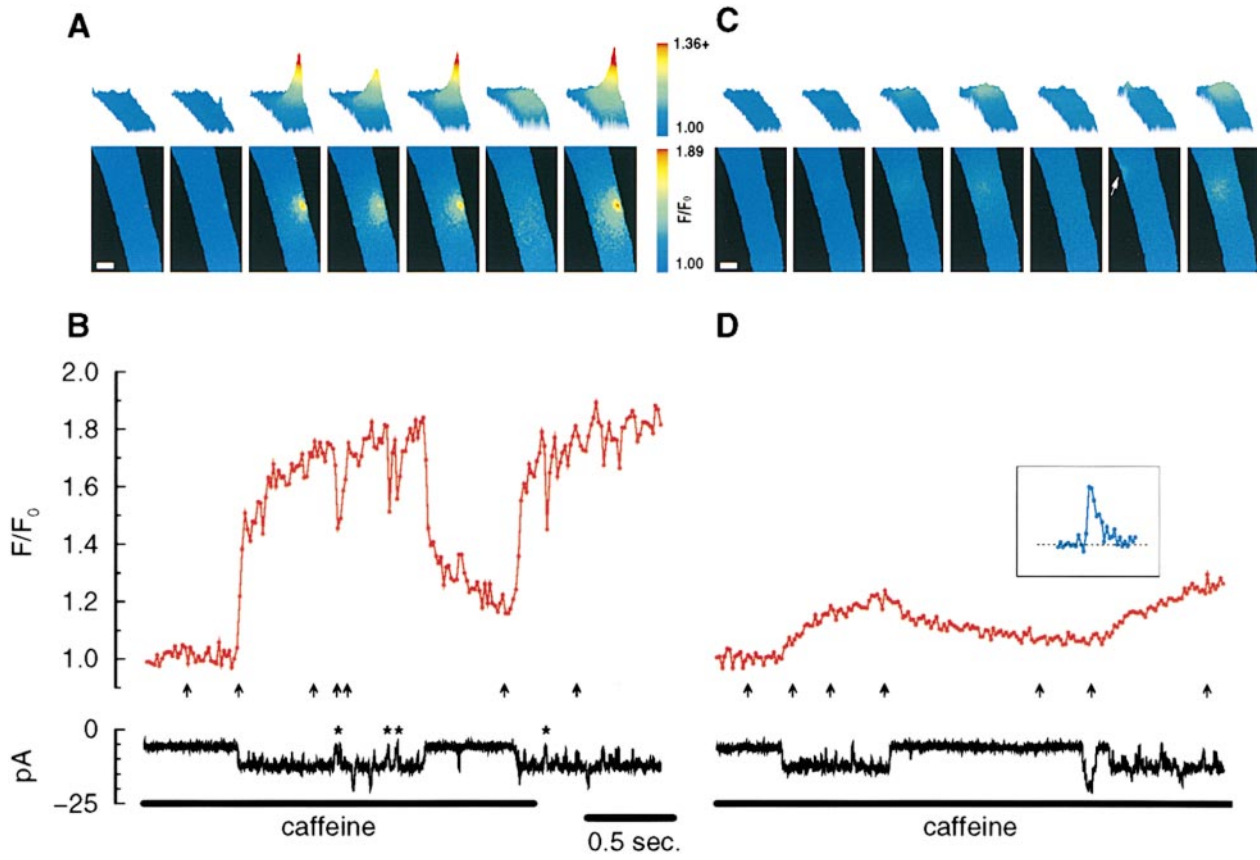

Figure 5. Compared with out-of-focus SCCaFTs, the fluorescence change from in-focus SCCaFTs has a larger amplitude, a more rapid initial rise and fall when the channel opens and closes, and a more punctate spatial spread in appearance when the channel initially opens, followed by a steeper spatial gradient. A and C show fluorescence images of SCCaFTs in the same cell at different times. Displayed above these selected images are the corresponding spatial profiles of fluorescence intensity. These profiles are slightly tilted so that the fluorescence distribution can be better visualized. The SCCaFT in A was more punctate in appearance when the channel opened initially (second image) and developed a steep spatial gradient during the slower rise (third, fifth, and seventh images). Both the increase and decrease of the fluorescence (corresponding to the opening and closing of the channel, respectively) clearly demonstrated a rapid and a slower phase (B). Brief closures of the channel (examples indicated by the stars above the current trace) resulted in brief decreases (or "valleys") in the fluorescence trace (primarily due to the rapid phases). A longer closure (~0.5 s in duration, beginning ~1.7 s into the record) reveals both the rapid and slow phases of the transient decrease. A brief opening (10 ms) during this closure causes a "spark-like" fast rise-and-fall (or a "peak") in the slowly decreasing fluorescence trace. In contrast, the SCCaFTs in C and D appear quite different. Based on the computer simulation in Fig. 4 and the images, the SCCaFTs in A are in focus or nearly in focus, while the long SCCaFTs in C are considerably out of focus. There was a briefer opening (~45 ms duration) of another channel that gave rise to the spark-like SCCaFT in the next-to-the-last image in C (at the arrowhead) and the inset in D (same fluorescence scale with $F/F_0 = 1$ indicated by the dotted line). This SCCaFT is more in focus than the longer SCCaFT. The full width at half-maximum at 15 ms for six SCCaFTs at the location of the one in A is 2.2 ± 0.2 μm (mean ± SEM, along the long axis). The beginning of the caffeine application was ~3 s before the trace in B and ~1 s before the trace in D. The channels that caused the additional openings in the current traces, other than those discussed above, are presumably out of the field. Pixel size for the images was 333 nm and the images were acquired every 15 ms. The scale bars are 5 μm in A and C.

in-focus SCCaFT has a more limited or punctate-appearing spatial spread when the channel initially opens, and a steeper spatial gradient throughout the opening (Fig. 5, A and C).

DISCUSSION

This study, to our knowledge, is the first to report the imaging of the localized fluorescence transient due to Ca^{2+} entry through a verifiable single opening of an ion channel. Using fluo-3 as a fluorescent Ca^{2+} indicator and a plasma membrane Ca^{2+}-permeable cation channel, it is possible to simultaneously record this transient (SCCaFT) and the unitary current at physiological extracellular Ca^{2+} concentrations.

Wide-Field Microscopy Permits SCCaFTs to be Detected Anywhere in the Cell Allowing Channel Localization

Because the wide-field microscope collects fluorescence from outside the focal plane of the camera in addition to the in-focus fluorescence, it is possible to detect the fluorescence transients anywhere in any plane within the image field. This is helpful for these studies because the location of the channels is not known before recording begins, and they do not appear to have a defined distribution pattern, as is the case for the sites of Ca^{2+} sparks in cardiac cells (Shacklock et al., 1995; Cheng et al., 1996; Parker et al., 1996). Moreover, imaging Ca^{2+} entry through openings of Ca^{2+}-permeable ion channels with a wide-field microscope provides a method for the determination of channel location in a manner similar to that used to locate mechanically gated channels in hair cells, though with different optical methods (Denk et al., 1995; Lumpkin and Hudspeth, 1995).

For the caffeine-activated channels in toad stomach smooth muscle cells, the channel appears to be randomly located in the plasma membrane (Fig. 1). In addition, multiple SCCaFTs often appear at the same location in one image set, and multiple image sets reveal a sparse SCCaFT distribution. These observations, plus the observation that only ~10–15 channels are open at the same time during maximal activation with caffeine (Guerrero et al., 1994a), suggest that rather than having a low probability of being open these channels have a low density on the plasma membrane. However, the possibility of closely clustered channels with (or without) some sort of local coordination of channel gating cannot be eliminated.

Comparing SCCaFTs with Sparks and Puffs/Blips

SCCaFTs reported here should not be confused with sparks or puffs/blips, which are the fluorescence transients reflecting localized increases in intracellular Ca^{2+} concentration due to Ca^{2+} release from intracellular Ca^{2+} stores through ryanodine or IP_3 receptors, respectively. These Ca^{2+} release events have usually been recorded with confocal line-scan imaging. Sparks have also been recorded in toad stomach smooth muscle cells with the same wide-field imaging system used here (ZhuGe et al., 1999). However, the sparks observed in these smooth muscle cells were much shorter in duration (rise time ~20 ms) and smaller in amplitude than SCCaFTs (presumably due to briefer underlying channel openings and possibly a smaller current) and, unlike SCCaFTs, could be detected in the absence of extracellular Ca^{2+} and were abolished when Ca^{2+} uptake into intracellular stores was blocked by the presence of thapsigargin (ZhuGe et al., 1998, 1999). Moreover, SCCaFTs were always associated with the openings of a plasma membrane channel.

Brief SCCaFTs, due to short openings of plasma membrane cation channels, having mainly the fast phases of the fluorescence change (e.g., see Fig. 5), resemble sparks. This suggests that the major components of the spark (the rising phase and the first part of the falling phase) reflect the fast phases of fluorescence change. The slow rising phase is not usually observed when recording sparks because they are normally brief events and there is little time for Ca^{2+} and Ca^{2+}-bound fluo-3 to diffuse further away before the channels close. A slow falling phase is also seen in some sparks. However, it is difficult to make exact comparisons because it is unclear how many ryanodine receptors are involved in spark formation and how well their openings and closings are synchronized, if indeed multiple channel openings are involved (see Schneider, 1999).

The SCCaFTs associated with long openings of the caffeine-activated channel in toad cells show some similarity to the prolonged sparks sometimes recorded when there were "modal changes in spark activity" (Parker and Wier, 1997) or when the underlying ryanodine receptors were presumably in a long duration conductance state in the presence of ryanodine (Cheng et al., 1993), imperatoxin A (Schneider, 1999; Shtifman et al., 1999), or FK506 (Xiao et al., 1997).

Arguments similar to the above can also be made for puffs and blips that occur with the opening of IP_3 receptors. The variation in the rising and falling phases of puffs (Sun et al., 1998), assuming they were all in focus, indicates asynchronous openings and closings of IP_3 receptors, in agreement with puffs being due to the opening of a cluster of IP_3 receptors. Moreover, the time course of the fluorescence change for certain prolonged blips resembles that of SCCaFTs (see Figure 5 in Sun et al., 1998).

Computer-simulated SCCaFTs Qualitatively Matched the Experimental Observations

The parameters used in the computer simulation of events underlying SCCaFTs (Fig. 4) were adopted from

the literature. Changes in these parameters did not qualitatively affect the fluorescence transient obtained from the simulation. However, there were quantitative effects. For example, decreasing the concentration of the stationary buffer or increasing the unitary current increased the initial rate of rise and the amplitude of the SCCaFT; increasing the resting Ca^{2+} concentration or cell diameter (resulting in an apparent increase in F_0)

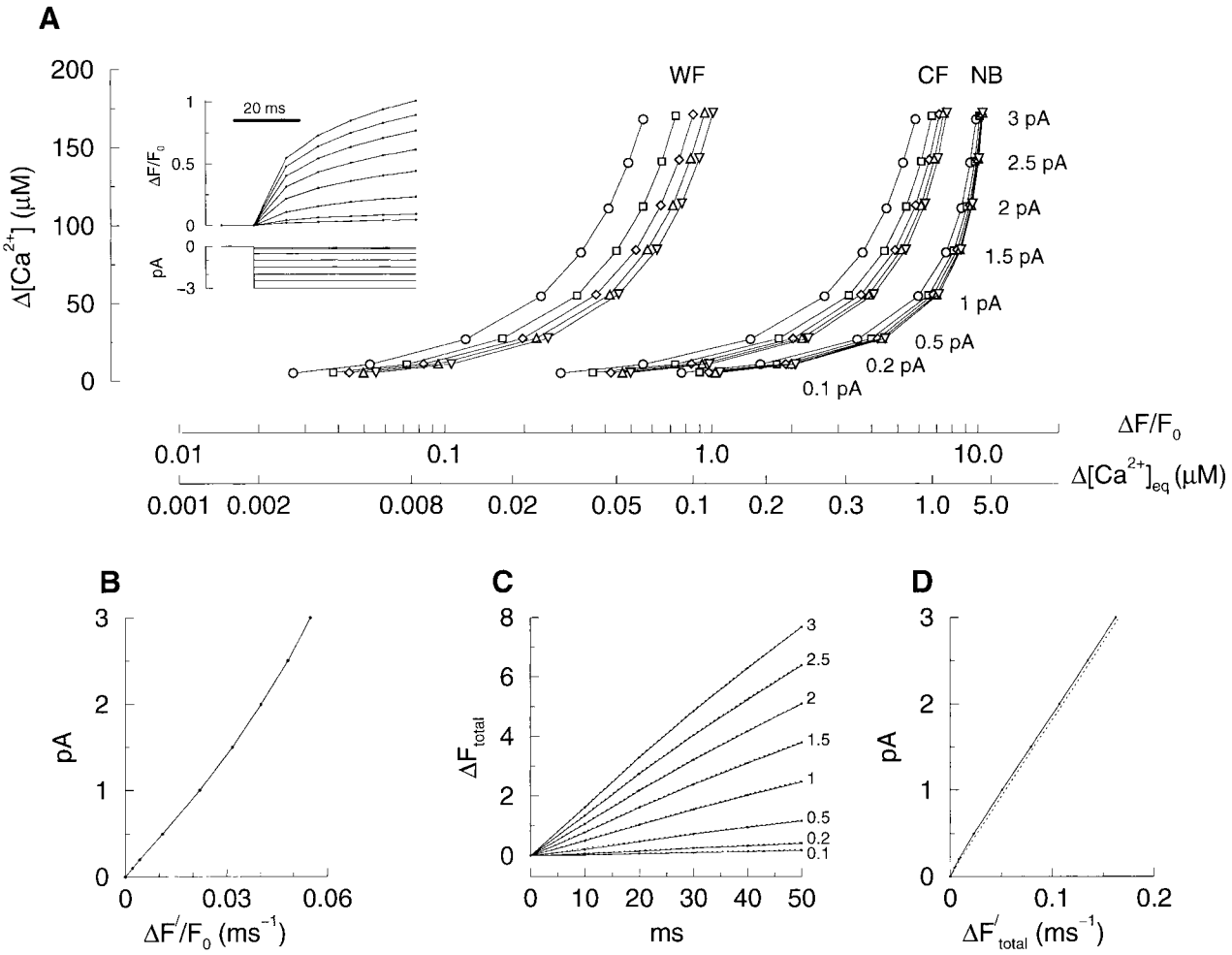

Figure 6. The relationship between the fluorescence transient and the underlying Ca^{2+} transient or Ca^{2+} current. Using the same approach and parameters as for the simulation in Fig. 4, fluorescence changes were generated for a series of Ca^{2+} currents varying from 0.1 to 3 pA. The blurred fluorescence changes (from a 100-nm square pixel overlaying the channel) were obtained using the point-spread function of a wide-field (A, inset) and that of a confocal microscope (traces not shown). The relationship between the observed in-focus fluorescence change ($\Delta F/F_0$, horizontal axis) for the wide-field microscope (labeled WF) and the underlying free Ca^{2+} concentration change ($\Delta[Ca^{2+}]_i$, vertical axis) obtained in a 100-nm voxel encompassing the channel is shown in A. The fluorescence measurements at 10 (○), 20 (□), 30 (◇), 40 (△), and 50 (▽) ms after the channel opened are plotted from left to right for each current (with the current labeled on the right). The horizontal axis indicates $\Delta F/F_0$ as well as the calculated change in free Ca^{2+} concentration assuming equilibrium ($\Delta[Ca^{2+}]_{eq} = [Ca^{2+}]_{eq} - [Ca^{2+}]_{rest}$) using the formula from Cheng et al. (1993): $[Ca^{2+}]_{eq} = K_d \cdot R/\{(K_d/[Ca^{2+}]_{rest} + 1) - R\}$, where $R = F/F_0$, $[Ca^{2+}]_{eq}$ is the free equilibrium Ca^{2+} concentration and $[Ca^{2+}]_{rest} = 0.1$ μM is the resting Ca^{2+} concentration. Also shown in A is the same relationship derived for a theoretical confocal microscope (CF) and for the changes in nonblurred fluorescence (Ca^{2+}-bound fluo-3 concentration, NB). For all three cases, the free Ca^{2+} concentration change (from the simulation, vertical axis) corresponding to each fluorescence change is much greater than that predicted using equilibrium considerations. Moreover, for the same underlying change in free Ca^{2+} concentration, the fluorescence signal is smaller for the wide-field microscope than for the confocal microscope. (B) The initial rate of rise (for the first 10 ms) of the in-focus fluorescence change ($\Delta F'/F_0$, where $\Delta F' = \Delta F/\Delta t$) at the pixel overlaying the channel from a wide-field microscope is nearly linearly related to the underlying Ca^{2+} current. C shows the time course of the total fluorescence increase (ΔF_{total}, within an 8-μm square that was large enough to collect the total fluorescence change) generated by 0.1–3 pA Ca^{2+} currents (labeled on the right). The solid lines and dotted lines represent the total fluorescence change for the in-focus and 2-μm out-of-focus images, respectively. The time course of the total fluorescence obtained from in- and out-of-focus images is essentially the same. Thus, the total fluorescence is essentially independent of focus. (D) Whether the fluorescence transient is in or out of focus, the rate of total fluorescence increase ($\Delta F'_{total} = \Delta F_{total}/\Delta t$, shown for the first 10 ms) is nearly linearly related to the Ca^{2+} current.

decreased the amplitude of the SCCaFT; decreasing the on and off rates of the stationary buffer (keeping K_d constant) increased the initial rate of rise and fall of the simulated SCCaFT. In general, these changes did not affect the overall shape of the fluorescence traces, all showed a rapid initial rise followed by a slower rise during channel opening and a rapid fall followed by a slower fall after the channel closed. The results of the simulation were also in agreement with other aspects of the observed fluorescence trace, such as a slower initial rate of rise and a smaller amplitude when the SCCaFT was out of focus.

Relationships Among the Change in Fluorescence, the Change in Free Ca^{2+} Concentration and the Underlying Ca^{2+} Current

Fluorescence transients have been used by others to obtain estimates of the free Ca^{2+} concentration change (or Ca^{2+} transient) and the underlying Ca^{2+} influx (or Ca^{2+} current). Shown in Fig. 6 A are the relationships between the measured fluorescence change and the free Ca^{2+} concentration change based on either the assumption that fluo-3 is in equilibrium with Ca^{2+} (see equation in Fig. 6 legend) or the simulation used for Fig. 4. The simulation is not constrained by the equilibrium assumption, which is invalid within nanometers of the open channel (Stern, 1992; Neher, 1998). From the simulation, given the same underlying Ca^{2+} transient (or current), an in-focus fluorescence transient observed with a confocal microscope is always larger than that observed with a wide-field microscope, and both are smaller than would be observed without blurring (Fig. 6 A). Thus, the greater the optical blurring the smaller the recorded fluorescence transient. Moreover, the free Ca^{2+} concentration (i.e., Ca^{2+} transient) at any $\Delta F/F_0$ is grossly underestimated by assuming equilibrium conditions. Therefore, the relationship between fluorescence transients and Ca^{2+} transients is complex and cannot be uniquely determined without a set of underlying assumptions about Ca^{2+} handling and the point spread function of the microscope (see also, Stern, 1992; Neher, 1998; Smith et al., 1998).

Extrapolation from the time course of fluorescence change to the underlying Ca^{2+} current is even more complex. When trying to calculate the Ca^{2+} current simply from the peak amplitude of the fluorescence transient (for example, calculating the current passing through the ryanodine receptor from the amplitude of an observed spark), the result can vary significantly depending on how long after the onset of the transient the peak occurs (Fig. 6 A, inset). For this reason, the initial rate of rise of the fluorescence trace is a better measure of the Ca^{2+} influx (as shown in Fig. 6 B), but this measurement should be made with the fluorescence transient in focus because fluorescence changes at different rates in different focal planes (see Fig. 4 C).

To avoid the requirement of imaging the fluorescence transients in focus as stated in the previous paragraph, the fluorescence change at any time on the rising phase can be spatially integrated over the image. As shown in Fig. 6 C, when the area of integration is large enough, the total fluorescence change is essentially the same whether the channel is in focus or 2 μm out of focus. The Ca^{2+} current can be determined from the rate of rise of the total fluorescence (Fig. 6 D). This is similar to the insightful approach used by Sun et al. (1998), who estimated the total Ca^{2+} release underlying Ca^{2+} puffs and blips by integrating the one-dimensional confocal linescan profile over three dimensions (the "signal mass"). In our case, the integration can be obtained directly from the two-dimensional wide-field images.

While this seems to be an appealing way for calculating Ca^{2+} current from the fluorescence measurement, it still has its limitations. Ca^{2+} removal and transport systems, as well as the concentrations of free Ca^{2+} and Ca^{2+} bound to buffers other than the fluorescent indicator, still need to be taken into account (as for any of these methods). In the absence of a detailed description of Ca^{2+} handling, these experiments would best be done with higher concentrations of Ca^{2+} indicator to capture more of the Ca^{2+} influx and/or by recording SCCaFTs and fluorescence events in the same cell or cell type. Then, the known current underlying the SCCaFT can be used to estimate the unknown currents giving rise to the other fluorescence events. The estimates will be more accurate if SCCaFTs and the fluorescence events are recorded at high imaging frequency, occur near the same location, and have close to the same rate of rise of fluorescence. The last can be adjusted by changing the underlying SCCaFT Ca^{2+} current by altering the Ca^{2+} driving force.

From the above discussion, as an example, an estimate of the Ca^{2+} current underlying Ca^{2+} sparks in toad stomach smooth muscle cells can be obtained using the fluorescence measurement from SCCaFTs. The initial rate of rise of fluorescence for the in-focus SCCaFTs from the cell in Fig. 5 is ~1.7%/ms (average of five transients), corresponding to a 1.4-pA Ca^{2+} current, assuming that 20% of the current was carried by Ca^{2+}. The initial rate of rise of a spark is ~1%/ms for a spark rise time of 20-ms with a 20% fluorescence increase (ZhuGe et al., 1998; Figures 2 and 4 in ZhuGe et al., 1999). Therefore, based on the near-linear relationship between the initial rate of rise of fluorescence and the Ca^{2+} current (Fig. 6 B), and neglecting the effect of any Ca^{2+} removal process, the Ca^{2+} current underlying the spark should be ~0.8 pA (≈1.4 pA × 1%/1.7%). If the ryanodine receptor in toad stomach smooth muscle cells has similar properties as those described by Mejía-Alvarez et al. (1999), this result would suggest that approximately three ryanodine receptors underlie the spark. A more

precise estimate requires a more complete data set. Moreover, systematic studies should be carried out using the "signal mass" or spatial integration (taking advantage of the near-linear relationship in Fig. 6 D).

The applicability of these methods is dependent upon the assumption that the fluorescence events (for example, sparks) are caused either by a single channel opening or by well synchronized openings of a few tightly clustered channels. If this does not occur or if there are brief channel closures, then the current determined in this way would be the average current.

We thank Jeff Carmichael, Rebecca McKinney, Brian Packard, Paul Tilander, and Yu Yan for excellent technical assistance; Karl Bellvé for the customized software used for this study; Stephen Baker for help with the statistical analysis; Robert Drummond and Michael Kirber for helpful advice and discussion as well as providing comments on earlier versions of this manuscript; and Fred Fay (deceased 18 March 1997) for the vision to apply and the wherewithal to develop digital imaging techniques for answering cell biological questions.

This work was supported in part by a National Institutes of Health program project grant HL47530 and National Science Foundation instrumentation grants DBI9200027 and DBI9724611.

Submitted: 26 April 1999 Revised: 28 July 1999 Accepted: 10 August 1999

REFERENCES

Berridge, M.J. 1997. Elementary and global aspects of calcium signaling. *J. Physiol.* 499:291–306.

Bers, D., C. Patton, and R. Nuccitelli. 1994. A practical guide to the study of Ca^{2+} in living cells. *In* Methods in Cell Biology. Vol. 40. R. Nuccitelli, editor. Academic Press, San Diego, CA. 3–29.

Blatter, L.A., J. Hüser, and E. Ríos. 1997. Sarcoplasmic reticulum Ca^{2+} release flux underlying Ca^{2+} sparks in cardiac muscle. *Proc. Natl. Acad. Sci. USA.* 94:4176–4181.

Blumenfeld, H., L. Zablow, and B. Sabatini. 1992. Evaluation of cellular mechanisms for modulation of calcium transients using a mathematical model of fura-2 Ca^{2+} imaging in *Aplysia* sensory neurons. *Biophys. J.* 63:1146–1164.

Bootman, M.D., M.J. Berridge, and P. Lipp. 1997a. Cooking with calcium: the recipes for composing global signals from elementary events. *Cell*. 91:367–373.

Bootman, M., E. Niggli, M. Berridge, and P. Lipp. 1997b. Imaging the hierarchical Ca^{2+} signaling system in HeLa cells. *J. Physiol.* 499:307–314.

Cannell, M.B., and C. Soeller. 1999. Mechanisms underlying calcium sparks in cardiac muscle. *J. Gen. Physiol.* 113:373–376.

Cheng, H., W.J. Lederer, and M.B. Cannell. 1993. Calcium sparks: elementary events underlying excitation–contraction coupling in heart muscle. *Science.* 262:740–744.

Cheng, H., M.R. Lederer, W.J. Lederer, and M.B. Cannell. 1996. Calcium sparks and $[Ca^{2+}]_i$ waves in cardiac myocytes. *Am. J. Physiol.* 270:C148–C159.

Denk, W., J.R. Holt, G.M.G. Shepherd, and D.P. Corey. 1995. Calcium imaging of single stereocilia in hair cells: localization of transduction channels at both ends of tip links. *Neuron*. 15:1311–1321.

Fay, F.S., R. Hoffman, S. LeClair, and P. Merriam. 1982. Preparation of individual smooth muscle cells from the stomach of *Bufo marinus*. *Methods Enzymol.* 85:284–291.

Guerrero, A., F.S. Fay, and J.J. Singer. 1994a. Caffeine activates a Ca^{2+}-permeable nonselective cation channel in smooth muscle cells. *J. Gen. Physiol.* 104:375–394.

Guerrero, A., J.J. Singer, and F.S. Fay. 1994b. Simultaneous measurement of Ca^{2+} release and influx into smooth muscle cells in response to caffeine: a novel approach for calculating the fraction of current carried by calcium. *J. Gen. Physiol.* 104:395–422.

Harkins, A.B., N. Kurebayashi, and S.M. Baylor. 1993. Resting myoplasmic free calcium in frog skeletal muscle fibers estimated with fluo-3. *Biophys. J.* 65:865–881.

Kargacin, G., and F.S. Fay. 1991. Ca^{2+} movement in smooth muscle cells studied with one- and two-dimensional diffusion models. *Biophys. J.* 60:1088–1100.

Klein, M.G., H. Cheng, L.F. Santana, Y.-H. Jiang, W.J. Lederer, and M.F. Schneider. 1996. Two mechanisms of quantized calcium release in skeletal muscle. *Nature.* 379:455–458.

Koizumi, S., M.D. Bootman, L.K. Bobanovic, M.J. Schell, M.J. Berridge, and P. Lipp. 1999. Characterization of elementary Ca^{2+} release signals in NGF-differentiated PC12 cells and hippocampal neurons. *Neuron*. 22:125–137.

Lassignal, N.L., J.J. Singer, and J.V. Walsh, Jr. 1986. Multiple neuropeptides exert a direct effect on the same isolated single smooth muscle cell. *Am. J. Physiol.* 250:C792–C798.

Lipp, P., and E. Niggli. 1996. A hierarchical concept of cellular and subcellular Ca^{2+}-signaling. *Prog. Biophys. Mol. Biol.* 65:265–296.

Lumpkin, E.A., and A.J. Hudspeth. 1995. Detection of Ca^{2+} entry through mechanosensitive channels localizes the site of mechanoelectrical transduction in hair cells. *Proc. Nat. Acad. Sci. USA.* 92:10297–10301.

Mejía-Alvarez, R., C. Kettlun, E. Ríos, M. Stern, and M. Fill. 1999. Unitary Ca^{2+} current through cardiac ryanodine receptor channels under quasi-physiological ionic conditions. *J. Gen. Physiol.* 113:177–186.

Naraghi, M., and E. Neher. 1997. Linearized buffered Ca^{2+} diffusion in microdomains and its implications for calculation of $[Ca^{2+}]$ at the mouth of a calcium channel. *J. Neurosci.* 17:6961–6973.

Neher, E. 1998. Vesicle pools and Ca^{2+} microdomains: new tools for understanding their roles in neurotransmitter release. *Neuron*. 20:389–399.

Nelson, M.T., H. Cheng, M. Rubart, L.F. Santana, A.D. Bonev, H.J. Knot, and W.J. Lederer. 1995. Relaxation of arterial smooth muscle by calcium sparks. *Science.* 270:633–637.

Parker, I., W.-J. Zang, and W.G. Wier. 1996. Ca^{2+} sparks involving multiple Ca^{2+} release sites along Z-lines in rat heart cells. *J. Physiol.* 497:31–38.

Parker, I., and Y. Yao. 1996. Ca^{2+} transients associated with openings of inositol trisphosphate-gated channels in *Xenopus oocytes*. *J. Physiol.* 491:663–668.

Parker, I., and W.G. Wier. 1997. Variability in frequency and characteristics of Ca^{2+} sparks at different release sites in rat ventricular myocytes. *J. Physiol.* 505:337–344.

Schneider, M.F. 1999. Ca^{2+} sparks in frog skeletal muscle: genera-

tion by one, some, or many SR Ca^{2+} release channels? *J. Gen. Physiol.* 113:365–371.

Shacklock, P.S., W.G. Wier, and C.W. Balke. 1995. Local Ca^{2+} transients (Ca^{2+} sparks) originate at transverse tubules in rat heart cells. *J. Physiol.* 487:601–608.

Shirokova, N., A. González, W.G. Kirsch, E. Ríos, G. Pizarro, M.D. Stern, and H. Cheng. 1999. Calcium sparks: release packets of uncertain origin and fundamental role. *J. Gen. Physiol.* 113:377–384.

Shtifman, A., C.W. Ward, H.H. Valdivia, and M.F. Schneider. 1999. Induction of long duration Ca^{2+} release events by imperatoxin A in frog skeletal muscle. *Biophys. J.* 76:A465. (Abstr.)

Smith, G.D., J.E. Keizer, M.D. Stern, W.J. Lederer, and H. Cheng. 1998. A simple numerical model of calcium spark formation and detection in cardiac myocytes. *Biophys. J.* 75:15–32.

Stern, M.D. 1992. Buffering of calcium in the vicinity of a channel pore. *Cell Calc.* 13:183–192.

Sun, X.-P., N. Callamaras, J.S. Marchant, and I. Parker. 1998. A continuum of $InsP_3$-mediated elementary Ca^{2+} signaling events in *Xenopus oocytes*. *J. Physiol.* 509:67–80.

Tella, L.L. 1985. The determination of a microscope's three-dimensional transfer function for use in image restoration. Master's Thesis, Worcester Polytechnic Institute, Worcester, MA.

Tsugorka, A., E. Ríos, and L.A. Blatter. 1995. Imaging elementary events of calcium release in skeletal muscle cells. *Science.* 269: 1723–1726.

Xiao, R.-P., H.H. Valdivia, K. Bogdanov, C. Valdivia, E.G. Lakatta, and H. Cheng. 1997. The immunophilin FK506-binding protein modulates Ca^{2+} release channel closure in rat heart. *J. Physiol.* 500:343–354.

Yao, Y., J. Choi, and I. Parker. 1995. Quantal puffs of intracellular Ca^{2+} evoked by inositol trisphosphate in *Xenopus* oocytes. *J. Physiol.* 482:533–553.

ZhuGe, R., R.A. Tuft, K.E. Fogarty, and J.V. Walsh, Jr. 1998. Coupling of voltage-activated Ca^{2+} channels with Ca^{2+} sparks and Ca^{2+} transients in smooth muscle. *J. Gen. Physiol.* 111:13a. (Abstr.)

ZhuGe, R., R.A. Tuft, K.E. Fogarty, K. Bellvé, F.S. Fay, and J.V. Walsh, Jr. 1999. The influence of sarcoplasmic reticulum Ca^{2+} concentration on Ca^{2+} sparks and spontaneous transient outward currents in single smooth muscle cells. *J. Gen. Physiol.* 113: 215–228.